Accounting for finite coherence in the analysis of dye sensitized solar cells and other thin film optoelectronic devices

Mayank Kumar Chaudhari*

Department of Physics, Indian Institute of Technology (BHU), Varanasi, Uttar Pradesh 221005, India

Current affiliation: Faculty of Physical Sciences, INSH, SRM University, Lucknow, Uttar Pradesh 225003, India

*Corresponding author: mayank.chaudhari.app09@itbhu.ac.in

The optical properties of thin films are governed by coherent optics rather than geometrical optics. For this reason various approaches based on coherent optics such as transfer matrix formulation are used extensively to study various thin film optoelectronic devices. Some thin film devices such as dye sensitized solar cells have layers which are thicker than the coherence length of light. Such a system having mixture of optically thin and optically thick media cannot be appropriately described either by coherent optics or ray optics alone. We formulate a framework based on coupled coherent and ray optics to account for finite coherence in modeling optical properties for thin film optoelectronics. We found that the optical response of the dye sensitized solar cell computed with coupled approach presented in this work shows better agreement with experimental results than that computed by transfer matrix formulation.

OCIS codes: 310.6860, 030.1670, 050.5298, 080.1753, 350.6050

1. Introduction

Dye sensitized solar cells (DSCs) are explored extensively in past few decades [1–6]. The incredible research interest in DSCs is attributed mainly to their low cost, compatibility with flexible materials and ability to optimize different parts individually. Unlike semiconductor junction based solar cells, the basic processes namely light absorption, electron transport and hole transport is carried out by different materials in the DSCs thus giving flexibility to optimize each material separately for best performance [1]. Besides offering low cost advantage, thin film cells' flexibility and semitransparency makes them preferred choice for various applications such as window panes. Various challenges inherent in original design of dye sensitized solar cells such as liquid electrolyte which caused maintenance issues, need for strongly absorbing dyes and elimination of expensive components such as TCO and Pt coated electrodes are being addressed[7], [8]. Utilizing aforementioned flexibility in independent study of each component of DSCs researchers have explored and synthesized various dyes[9–11], various approaches have been proposed for improving efficiency of charge transport in TiO2 [12–15].

Approaches to enhance light harvesting efficiency (LHE) include photon confinement by brag reflectors and nano-tube structured TiO2 [16–20], use of diffuse scattering by introducing large-sized TiO2 particles [21,22] etc. The use of combined effect of scattering layer and photon confinement by Total Internal Reflections, later improved by use of directionally selective filters[23–25] have also been demonstrated both theoretically and practically by M. Peters' group.

The principle approaches used for theoretical study of thin film solar cells including DSCs are based on deterministic coherent optics model such as transfer matrix formulation [26, 27]. Computation of field intensity profiles, absorption depth profiles using transfer matrix formulation has been reported [27] and an approach to account for the parasitic absorptions in internal quantum efficiency measurements is proposed by Prof McGehee group [22]. Yet the modeling of diffused scattering or radiative recombination processes in thin film structures is rather unexplored. Sophie Wenger has reported the ray-tracing algorithm based framework for coupled optical and electrical model of DSCs in which the optical properties of thin films are computed separately by transfer matrix formulation and the rest of the system is treated with ray-tracing algorithm [28]. We have formulated a more flexible algorithm based on similar coupled coherent and geometrical approach to analyze effects of finite coherence on DSCs equipped with brag reflector. Our approach does not involve ray tracing and thus it is computationally very efficient. Unlike the ray tracing based approach, we are able to compute normalized field intensity profile and absorption depth profile as well. Thus, we can account for parasitic absorption and compute photo-generation as a function of position in the device for both thin films and thick layers.

Although coherence properties of light are statistical in nature rather than being deterministic and more so when the coherence length of light is being altered by interactions with layered media, the study of interplay between coherent and geometrical optics governing the optical characteristics of layered media composed of thin films and the layers having thicknesses considerably greater than coherence length of incident light based on deterministic optical models can help explain the characteristics of layered media more accurately. Along with that it also provides a way to analyze characteristics of the thin films when under angularly selective filters such as Rugate filters on top of thick glass substrate. An efficient, highly flexible and robust approach based on combined coherent and geometrical optics has been presented here for precise modeling of DSCs and other thin film optoelectronic devices.

2. Coupled Coherent and Geometrical Optics Approach

The layered media comprising of optically thin layers (sufficiently thinner than coherence length of incident light) and optically thick layers, often encountered in thin film solar cells such as DSCs, can be modeled more accurately by first treating the identified thin films with coherent approach and then using the result to study the system as a whole with geometrical optics [28]. Layers such as glass substrates, electrolyte layer and sometimes the photo-anode in DSCs are typically much thicker than coherence length of sunlight and cannot be accurately modeled with coherent approach. Whereas the layers such as anti-reflective coating TCO and the layers comprising photonic crystal are much thinner and must be modeled with coherent approach to take into account the effects such as interference. In this section we first describe the theoretical model of DSCs and then explain the application of combined coherent and geometrical optics approach to analyze the model. In the next section we describe the results by comparing them with results obtained by transfer matrix approach and the practical results reported in the literature.

2.1. Modeling one-dimensional dye sensitized solar cell

We analyze the one-dimensional model of dye sensitized solar cell coupled with photonic crystal constructed by alternate layers of TiO2 and SiO2 repeated many times. Such models have been reported in literatures [26, 29–31]. The formulation of transfer matrix corresponding to each layer rather than each boundary allows implementation of any number of repetitions of layers without increasing computational cost. Here it is worth mentioning here that when light interacts with brag reflectors such as the one used in this model the coherent properties of light are changed considerably. In specific enhancement in coherence length for the wavelength for which the reflections from brag reflector are constructive can be seen using simple finite time domain visualization of fields. However, the intensity of enhanced coherence length is typically lowered significantly. In this approach we have neglected this effect. A more evolved approach accounting for statistical nature of coherent phenomena occurring in the system can be

formulated by incorporating statistical optics principles in the approach presented herein to explain the phenomena more accurately.

The schematic diagram of the theoretical model and working of DSCs is shown in fig. 1. DSCs can typically be fabricated by printing porous TiO_2 nanoparticle film on transparent conducting oxide (TCO) coated glass substrate simply by applying the TiO_2 nanoparticle paste. Some advanced techniques include atomic layer deposition[32], pre-treatment of photoanode with $TiCl_4$ [33], preparation of thick inverse opals through a multi-cycle process[20] etc. The dye is anchored to the TiO_2-nanoparticle mesh by placing the printed glass substrate in dye solution for prolonged time. The cell is then sealed after placing adequate spacers and liquid I-/I3- redox pair based electrolyte is injected to completely drench the dye coated TiO_2 photo-electrode. One dimensional photonic crystal can be created by depositing SiO_2 and TiO_2 successively after the dye has been adsorbed on the photoanode [26].

The parameters affecting the optical properties of such layered media are wavelength dependent refractive indices, the thicknesses of each layer and the arrangement or the ordering of the layers. Thus for use in this model each layer is characterized by its thickness and the wavelength dependent complex refractive index. The refractive indices are taken from literature. The refractive index of the photo-electrode n_{PE} is modeled by following equation.

$$n_{PE} = n_0 + a_0 \exp\left(1 - \xi(\lambda) - e^{-\xi(\lambda)}\right) i, \tag{1}$$

$$\text{Where, } \xi(\lambda) = (\lambda - \lambda_0) / \Delta\lambda$$

This model should serve as a reference to explain the coupled coherent and geometrical matrix approach. In the result and discussion section we have also presented the analysis of dye sensitized solar cells with anti-reflective coating layer and the cells having more than one absorbing layers to account for parasitic absorption.

2.2. Coupled coherent and geometric optics framework

At first place we identify the thin films and compute their reflection and transmission spectra by employing well-known transfer matrix formulation. For each layer transfer matrix can be formulated simply by applying boundary conditions requiring continuity of the components of fields parallel to the interfaces. The reflection and transmittance at the interface of two thick layers can be computed by Fresnel's equations. The reflection and transmission coefficients for transverse electric (TE) or s-polarization (R_s and T_s) and transverse magnetic (TM) or p-polarization (R_p and T_p) at an interface are given by following Fresnel's equations.

$$R_s = \left| \frac{n_1 \cos(\theta_i) - n_2 \cos(\theta_t)}{n_1 \cos(\theta_i) + n_2 \cos(\theta_t)} \right|^2$$

$$R_p = \left| \frac{n_1 \cos(\theta_t) - n_2 \cos(\theta_i)}{n_1 \cos(\theta_t) + n_2 \cos(\theta_i)} \right|^2$$

$$T_s = 1 - R_s; \quad T_p = 1 - R_p$$

θ_i and θ_t are the angle of incidence and transmission respectively and are related by Snell's law. Now the thin films in the structures can be treated as interfaces with reflection and transmission properties computed by transfer matrix formulation. Note that in general reflectance and transmittance is not complementary for these interfaces as light is absorbed by thin films as well. At this point we are ready to treat the resultant model with geometrical optics. In other words we are coupling the output of coherent model to the geometrical optics model.

2.2.1. Recursive algorithm for geometrical optics computation

Instead of using complex ray tracing algorithm we formulate an approach based on recursive or iterative algorithm. Just as we have computed reflection and transmittance spectra of thin films and then treated them as interface between two thick layers, we can even compute reflectance and transmission across a thick layer and then replace it by equivalent interface. The resulting system now is again a stack of thick layers, the input for next iteration. This kind of formulation allows us to use versatile iterative or recursive algorithm to compute optical properties of such layered media. Unlike ray tracing this approach provides greater flexibility and allows computation of field intensity and absorption depth profiles in both thin films and optically thick layers. Computational cost effectiveness will be evident from the description of the algorithm in subsequent discussion.

Firstly the total transmission and reflectance across one layer for incidence from both the top and bottom side (reflectance and transmittance across a layer for incidence from opposite directions is not always same, e.g., when we are dealing with layers involving lossy dielectrics) are computed for one layer and then the layer is represented by equivalent interface having optical properties defined by following relations.

$$R_{11} = r_{11} + \frac{t_{11} r_{21} \exp\left(-2\alpha d / \cos(\theta_t)\right) t_{12}}{1 - r_{12} r_{21} \exp\left(-2\alpha d / \cos(\theta_t)\right)}$$

$$T_{11} = \frac{t_{11} \exp\left(-\alpha d / \cos(\theta_t)\right) t_{21}}{1 - r_{12} r_{21} \exp\left(-2\alpha d / \cos(\theta_t)\right)}$$

$$R_{12} = r_{22} + \frac{t_{22} r_{12} \exp\left(-2\alpha d / \cos\left(\theta_t\right)\right) t_{21}}{1 - r_{21} r_{12} \exp\left(-2\alpha d / \cos\left(\theta_t\right)\right)}$$

$$T_{12} = \frac{t_{22} \exp\left(-\alpha d / \cos\left(\theta_t\right)\right) t_{12}}{1 - r_{21} r_{12} \exp\left(-2\alpha d / \cos\left(\theta_t\right)\right)}$$

Here, the first subscript is the index of the interface and second subscript denotes the direction of incidence. For example, the symbol r_{21} is used to represent the reflection coefficient of the 2nd interface when light is incident from the top and r_{12} is used to represent the reflection coefficient when light is incident on 1st interface from the bottom side. The symbols r_{ij}, t_{ij} represent the reflectance and transmittance of the interfaces for particular angle of incidence and polarization respectively, whereas the capital symbols R_{ij}, T_{ij} represent the reflectance and transmittance of the layer as a whole respectively or in other words it represents the properties of the equivalent interface created by collapsing this layer. θ_t is the angle of transmission and can be computed from Snell's law. The coefficient of absorption α is given by $\alpha = 4\pi Im(n)/\lambda$. Fig. 2 depicts multiple reflections and transmissions in the layered medium. The relations stated above can easily be derived by summing up intensities of individual reflections which is in the form of a geometric progression. Here it is worth mentioning that for geometrical optics considerations we simply add the intensities and thus account for absence of interference phenomena whereas in thin films the resultant is addition of amplitudes accounting for interference of electromagnetic waves reflected or transmitted by various interfaces in the system.

3. Results and Discussions

Firstly we demonstrate the effect of finite coherence properties of incident light on optical response of the layered structure. Comparison between fractions of light absorbed and reflected, the normalized field intensity profile as a function of position in the device (excluding electrolyte layer as it is too thick for proper representation) for selected wavelengths and the photo-generation rate for a DSC under normal illumination, when analyzed with transfer matrix approach and with coupled approach considering electrolyte and both electrolyte and working electrode as thick layers, is shown in figure 3. It is evident from these results that finite coherence length has a significant effect on the optical properties and performance of the cell. For further discussion we shall use the term case 1 to refer to simulation using only coherent optics, case 2 for simulation considering only electrolyte as thick layer and case 3 for simulation considering both electrolyte and working electrode as thick layers. As seen from figures 3(a), 3(b) and figure 4 LHE and reflectance for case 2 is as good as averaging of results for case 1. Generally this is not significant when compared to averaging effect due to imperfections in interfaces. Thus, the discrepancy between experimental results and theoretical modeling are explained by imperfection at interfaces. Or in other words, it does not make much sense when results for too thick layers using coherent

and geometrical approach are compared as there will be very large number of interference maxima and minima for same wavelength interval. However, when working electrode is considered thick, i.e. case 3, the results obtained are significantly different. The difference is more clearly seen for oblique incidence (fig. 4). The LHE is higher for oblique incidence as path length within active layer is significantly enhanced. The enhancement is reflectance is similar to that expected by Fresnel's equations. Normalized intensity profiles for different wavelengths as a function of position in the device are nearly same for case 1 and case 2 in the working electrode or active layer (fig. 3(c), (d), (e)) leading to same photogeneration rate profile for both case 1 and case 2 (fig. 3(f)). Attenuation of the incident beam is however not appreciable due to very low absorption coefficient of DSC under consideration. The normalized intensity profile also accounts for enhancement in LHE of the cell when coupled to a brag reflector [26].

The comparison between LHE and Reflectance for two DSCs with 7500 nm thick working electrode and 600 nm thick working electrode is shown in fig. 5. For DSC with 7500 nm thick working electrode all parameters are same as the DSC used for fig. 3 except the thickness of working electrode. For DSC with 600 nm thick working electrode, α_0 is taken to be 0.0055 and n_0 is taken to be 1.92. Moreover the thickness of SiO_2 layer is changes to 60 nm, while the thickness of TiO_2 is kept the same. We have deliberately used same parameters that are used by Gabriel Lozano [26] in order to compare the experimental and theoretical results and thus explain the effect of finite coherence length of light. When comparing our simulated results with experimental and theoretical results reported by Gabriel Lozano [26], we found that the experimental results for DSC having 600 nm thick working electrode agrees more closely with results obtained by treating working electrode as a part of thin film (case 2) whereas the experimental results for DSC with 7500 nm thick electrode agrees better with results obtained by treating both electrolyte and working electrode as thick layers (case 3). This is because coherence length of light is of the order of 8 to 10 wavelengths in case of sunlight, which is obviously much higher than 600 nm and comparable to 7500 nm. Thus, the effect of interference after reflections and refractions from multiple surfaces will be seen for 600 nm thick working electrode whereas such interference effects will be missing for 7500 nm thick electrode.

The thickness of electrolyte layer is obviously very large compared to coherence length of incident sunlight. Thus, certainly there will be no observable interference due to reflections and transmissions at interfaces bounding electrolyte layer. Variation of short circuit current under one sun illumination (AM1.5) with respect to angle of incidence assuming 100% internal quantum efficiency for the DSC with 7500 nm thick working electrode is shown in Fig. 6 and angular responses of the cell in terms of LHE and reflectance for wavelengths 600 nm, 550 nm and 400 nm are shown in Fig 7. As seen in fig. 6 short circuit

current increases with angle of incidence due to increased path length within the working electrode. However, increase in reflectance is more dominant above 75^0.

References

1. B. E. Hardin, H. J. Snaith, and M. D. McGehee, “The renaissance of dye-sensitized solar cells,” *Nat. Photon-*, vol. 6, pp. 162–169, 2012.
2. W. Tan, J. Chen, X. Zhou, J. Zhang, Y. Lin, X. Li, and X. Xiao, “Preparation of nanocrystalline TiO2 thin film at low temperature and its application in dye-sensitized solar cell,” vol. 13, no. 5. Springer-Verlag, 01-May-2009.
3. J. Chen, F.-Q. Bai, J. Wang, L. Hao, Z.-F. Xie, Q.-J. Pan, and H.-X. Zhang, “Theoretical studies on spectroscopic properties of ruthenium sensitizers absorbed to TiO2 film surface with connection mode for DSSC,” *Dyes Pigment.*, vol. 94, pp. 459–468, Sep. 2012.
4. L. Ke, S. B. Dolmanan, L. Shen, P. K. Pallathadk, Z. Zhang, D. M. Y. Lai, and H. Liu, “Degradation mechanism of ZnO-based dye-sensitized solar cells,” *Sol. Energy Mater. Sol. Cells*, vol. 94, pp. 323–326, Feb. 2010.
5. L. Jin, J. Zhai, L. Heng, T. Wei, L. Wen, L. Jiang, X. Zhao, and X. Zhang, “Bio-inspired multi-scale structures in dye-sensitized solar cell,” *J. Photochem. Photobiol. C: Photochem. Rev.*, vol. 10, pp. 149–158, 2009.
6. L. Kavan, N. Tétreault, T. Moehl, and M. Grätzel, “Electrochemical Characterization of TiO 2 Blocking Layers for Dye-Sensitized Solar Cells,” *J. Phys. Chem. C*, vol. 118, pp. 16408–16418, Jul. 2014.
7. Q. Dai, D. R. MacFarlane, P. C. Howlett, and M. Forsyth, “Rapid I?/I3?: Diffusion in a Molecular-Plastic-Crystal Electrolyte for Potential Application in Solid-State Photoelectrochemical Cells,” *Angew. Chem.*, vol. 117, pp. 317–320, Jan. 2005.
8. A. Mishra, M. K. R. Fischer, and P. Bäuerle, “Metal-free organic dyes for dye-sensitized solar cells: from structure: property relationships to design rules.,” *Angew. Chem.*, vol. 48, no. 14, pp. 2474–2499, 2009.
9. S. Mathew, A. Yella, P. Gao, R. Humphry-Baker, B. F. E. Curchod, N. Ashari-Astani, I. Tavernelli, U. Rothlisberger, M. K. Nazeeruddin, and M. Grätzel, “Dye-sensitized solar cells with 13% efficiency achieved through the molecular engineering of porphyrin sensitizers.,” *Nat. Chem.*, vol. 6, no. 3, pp. 242–247, 2014.
10. S. Ramkumar, S. Manoharan, and S. Anandan, “Synthesis of D-($\uppi$-A)2 organic chromophores for dye-sensitized solar cells,” *Dyes Pigment.*, vol. 94, pp. 503–511, Sep. 2012.
11. J.-J. Cid, J.-H. Yum, S.-R. Jang, M. K. Nazeeruddin, E. Martínez-Ferrero, E. Palomares, J. Ko, M. Grätzel, and T. Torres, “Molecular Cosensitization for Efficient Panchromatic Dye-Sensitized Solar Cells,” *Angew. Chem.*, vol. 119, pp. 8510–8514, Nov. 2007.
12. S. H. Ko, D. Lee, H. W. Kang, K. H. Nam, J. Y. Yeo, S. J. Hong, C. P. Grigoropoulos, and H. J. Sung, “Nanoforest of hydrothermally grown hierarchical ZnO nanowires for a high efficiency dye-sensitized solar cell.,” *Nano Lett.*, vol. 11, no. 2, pp. 666–671, 2011.
13. J. Shen, R. Cheng, Y. Chen, X. Chen, Z. Sun, and S. Huang, “A Novel TiO_2 Tape for Fabricating Dye-Sensitized Solar Cells on Universal Conductive Substrates,” *ACS Appl. Mater. & Interfaces*, vol. 5, no. 24, pp. 13000–13005, Dec. 2013.
14. K.-J. Jiang, J.-M. Zhou, K. Manseki, Q.-S. Liu, J.-H. Huang, Y. Song, and S. Yanagida, “Integration of High-Performance Nanocrystalline TiO 2 Photoelectrodes for N719-Sensitized Solar Cells,” *Int. J. Photoenergy*, vol. 2013, pp. 1–6, 2013.
15. M. M. Khan, S. A. Ansari, D. Pradhan, M. O. Ansari, D. H. Han, J. Lee, and M. H. Cho, “Band gap engineered TiO 2 nanoparticles for visible light induced photoelectrochemical and photocatalytic studies,” *J. Mater. Chem.*, vol. 2, pp. 637–644, 2014.
16. M. Guo, Z. Yong, K. Xie, J. Lin, Y. Wang, and H. Huang, “Enhanced Light Harvesting in Dye-Sensitized Solar Cells Coupled with Titania Nanotube Photonic Crystals: A Theoretical Study,” *ACS Appl. Mater. & Interfaces*, Dec. 2013.
17. M. R. Mohammadi, R. R. M. Louca, D. J. Fray, and M. E. Welland, “Dye-sensitized solar cells based on a single layer deposition of TiO2 from a new formulation paste and their photovoltaic

performance," *Sol. Energy*, vol. 86, pp. 2654–2664, Sep. 2012.
18. H. Wang, J. He, G. Boschloo, H. Lindström, A. Hagfeldt, and S.-E. Lindquist, "Electrochemical Investigation of Traps in a Nanostructured TiO_2 Film," *J. Phys. Chem. B*, vol. 105, no. 13, pp. 2529–2533, Mar. 2001.
19. S. I. Cha, K. H. Hwang, Y. H. Kim, M. J. Yun, S. H. Seo, Y. J. Shin, J. H. Moon, and D. Y. Lee, "Crystal splitting and enhanced photocatalytic behavior of TiO2 rutile nano-belts induced by dislocations," *Nanoscale*, vol. 5, no. 2, pp. 753–758, Dec. 2012.
20. C.-Y. Kuo and S.-Y. Lu, "Fabrication of a multi-scale nanostructure of TiO2 for application in dye-sensitized solar cells," *Nanotechnology*, vol. 19, 2008.
21. M. Patterson, S. Hughes, S. Combri'e, N.-V.-Q. Tran, A. D. Rossi, R. Gabet, and Y. Jaouen, "Disorder-induced coherent scattering in slow-light photonic crystal waveguides," *arXiv ePrints*, Jun. 2009.
22. G. F. Burkhard, E. T. Hoke, and M. D. McGehee, "Accounting for interference, scattering, and electrode absorption to make accurate internal quantum efficiency measurements in organic and other thin solar cells.," *Adv. Mater.*, vol. 22, no. 30, pp. 3293–3297, 2010.
23. M. Peters, J. C. Goldschmidt, T. Kirchartz, and B. Bläsi, "The photonic light trap—Improved light trapping in solar cells by angularly selective filters," *Sol. Energy Mater. Sol. Cells*, vol. 93, pp. 1721–1727, Oct. 2009.
24. M. Peters, J. C. Goldschmidt, and B. Bläsi, "Angular confinement and concentration in photovoltaic converters," *Sol. Energy Mater. Sol. Cells*, vol. 94, pp. 1393–1398, Aug. 2010.
25. M. Peters, C. Ulbrich, J. C. Goldschmidt, J. Fernandez, G. Siefer, and B. Bläsi, "Directionally selective light trapping in a germanium solar cell," *Opt. Express*, vol. 19. Optical Society of America (OSA), p. 136, 2011.
26. G. Lozano, S. Colodrero, O. Caulier, M. E. Calvo, and H. Mi´guez, "Theoretical Analysis of the Performance of One-Dimensional Photonic Crystal-Based Dye-Sensitized Solar Cells," *J. Phys. Chem. C*, vol. 114, pp. 3681–3687, Mar. 2010.
27. L. A. A. Pettersson, L. S. Roman, and O. Inganäs, "Modeling photocurrent action spectra of photovoltaic devices based on organic thin films," *J. Appl. Phys.*, vol. 86, 1999.
28. S. Wenger, M. Schmid, G. Rothenberger, A. Gentsch, M. Grätzel, and J. O. Schumacher, "Coupled Optical and Electronic Modeling of Dye-Sensitized Solar Cells for Steady-State Parameter Extraction," *J. Phys. Chem. C*, vol. 115, pp. 10218–10229, May 2011.
29. A. Mihi and H. Míguez, "Origin of Light-Harvesting Enhancement in Colloidal-Photonic-Crystal-Based Dye-Sensitized Solar Cells," *J. Phys. Chem. B*, vol. 109, pp. 15968–15976, Aug. 2005.
30. S. Colodrero, A. Mihi, J. A. Anta, M. O. a, and H. Míguez, "Experimental Demonstration of the Mechanism of Light Harvesting Enhancement in Photonic-Crystal-Based Dye-Sensitized Solar Cells," *J. Phys. Chem. C*, vol. 113, pp. 1150–1154, Jan. 2009.
31. S. Colodrero, A. Mihi, L. Häggman, M. Ocaña, G. Boschloo, A. Hagfeldt, and H. Míguez, "Porous One-Dimensional Photonic Crystals Improve the Power-Conversion Efficiency of Dye-Sensitized Solar Cells," *Adv. Mater.*, vol. 21, pp. 764–770, Feb. 2009.
32. D. Hess, M. Mushfiq, R. Dalvi, R. Winter, U. Sampathkumaran, K. Goswami, A. Yangaus-Gil, and J. W. Elam, "Dye-Sensitized Solar Cells Fabricated from Atomic Layer Deposited Photoanodes on Aerogel Scaffolds."
33. S. Ito, T. N. Murakami, P. Comte, P. Liska, C. Grätzel, M. K. Nazeeruddin, and M. Grätzel, "Fabrication of thin film dye sensitized solar cells with solar to electric power conversion efficiency over 10%," *Thin Solid Films*, vol. 516, pp. 4613–4619, May 2008.

Figure Captions

1. Schematic diagram of construction and working of a DSC.
2. Multiple reflections and transmissions within layered medium.
3. Absorption spectrum (a), reflectance spectrum (b), normalized intensity variation as a function of position in the device for 550 nm wavelength (c), 500 nm wavelength (d) and 460 nm wavelength (e), photogeneration rate as a function of position in the device (f) for a DSC depicted in fig 1, when under normal incidence, with following parameters: dTCO=400 nm, nTCO=1.8; working electrode characterized by a_0 = 0.004, $\Delta\lambda$ = 64.16 nm, λ_0 = 538 nm (see equation 1) and dWE = 1500 nm; photonic crystal realized by 3 layers of each SiO2 and TiO2 with refractive indices 1.43 and 1.92 respectively and thicknesses 95 and 80 respectively, place alternatively; Thickness and refractive index of electrolyte layer are 50 micron and 1.433 respectively; Light gray lines shows results obtained by considering entire cell with coherent optics, thin black line is used for representing results obtained by treating only the electrolyte layer as thick layer and the dark (thick) black line is used for results obtained by treating both electrolyte and working electrode as thick layers.
4. LHE (top) and reflectance (bottom) spectra when angle of incidence is 300 (TE mode). Light gray lines shows results obtained by considering entire cell with coherent optics, thin black line is used for representing results obtained by treating only the electrolyte layer as thick layer and the dark (thick) black line is used for results obtained by treating both electrolyte and working electrode as thick layers. All other parameters are same as in figure 3.
5. Comparison between LHE and Reflectance for DSC having 7500 nm thick working electrode (left) and DSC having 600 nm thick working electrode (right).
6. Variation of short circuit current with respect to angle of incidence. Broken gray lines shows results obtained by considering entire cell with coherent optics (case1), thin black line is used for representing results obtained by treating only the electrolyte layer as thick layer (case 2) and the dark (thick) black line is used for results obtained by treating both electrolyte and working electrode as thick layers (case 3).
7. Angular response in terms of LHE (top) and reflectance (bottom) for 600 nm (left), 550 nm (middle) and 400 nm (right) wavelengths.

Figures:

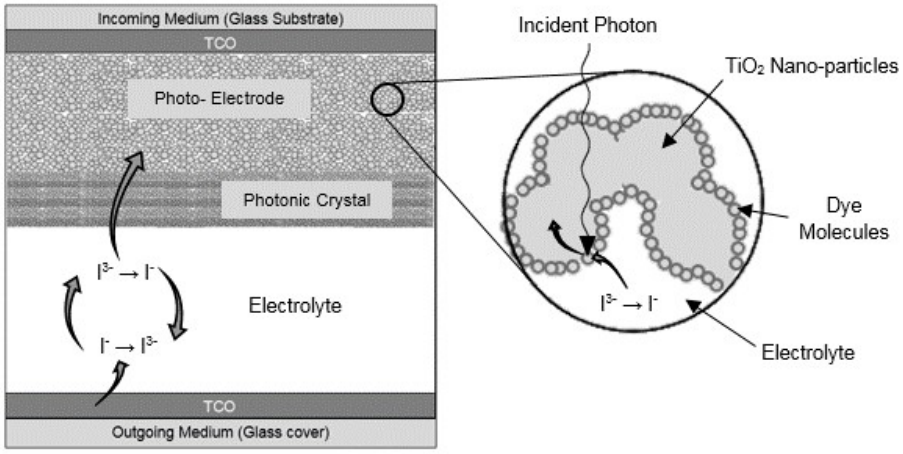

Fig. 1

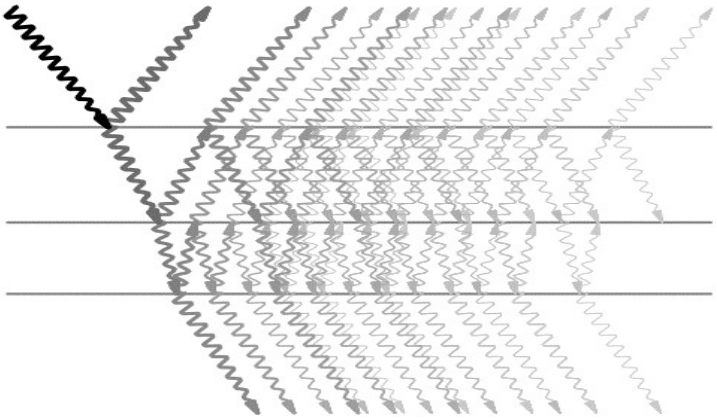

Fig. 2

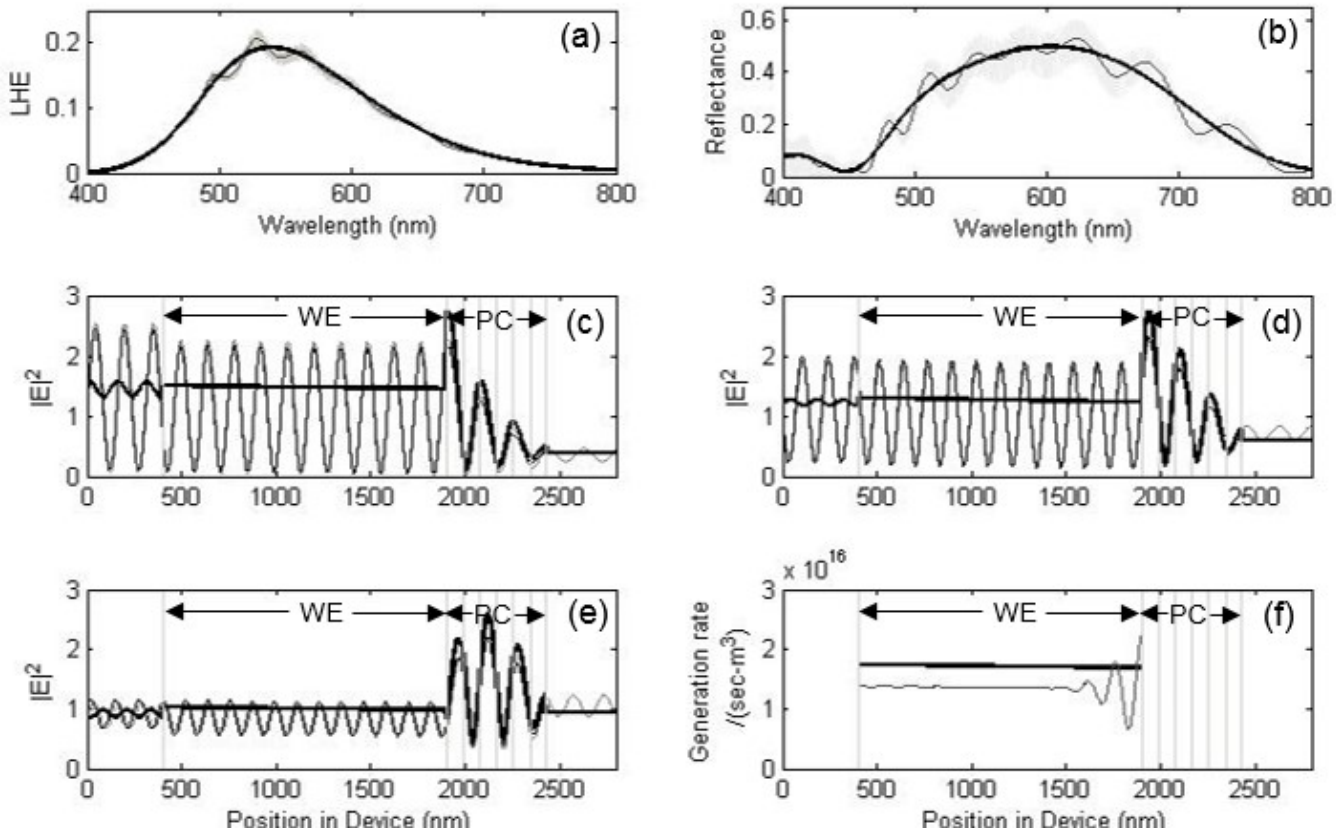
(a)
LHE
Wavelength (nm)
(b)
Reflectance
Wavelength (nm)
(c)
WE
PC
|E|2
(d)
WE
PC
|E|2
(e)
WE
PC
|E|2
Position in Device (nm)
(f)
x 10^16
WE
PC
Generation rate /(sec-m3)
Position in Device (nm)

Fig. 3

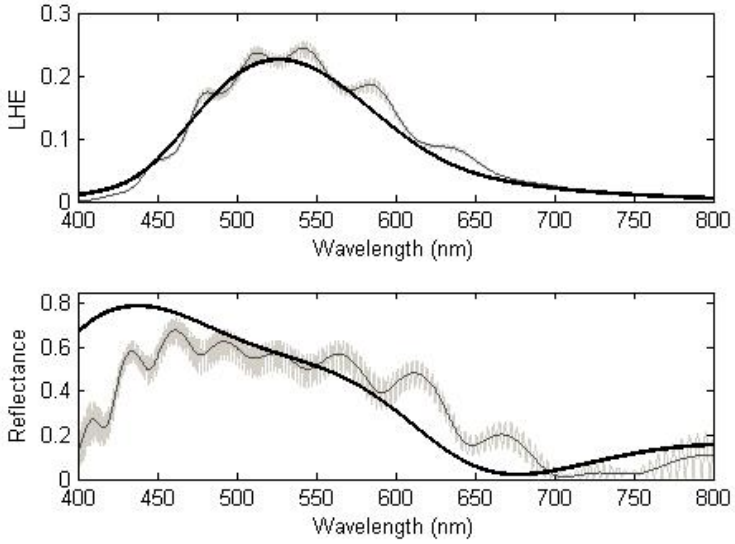
LHE
Wavelength (nm)
Reflectance
Wavelength (nm)

Fig. 4

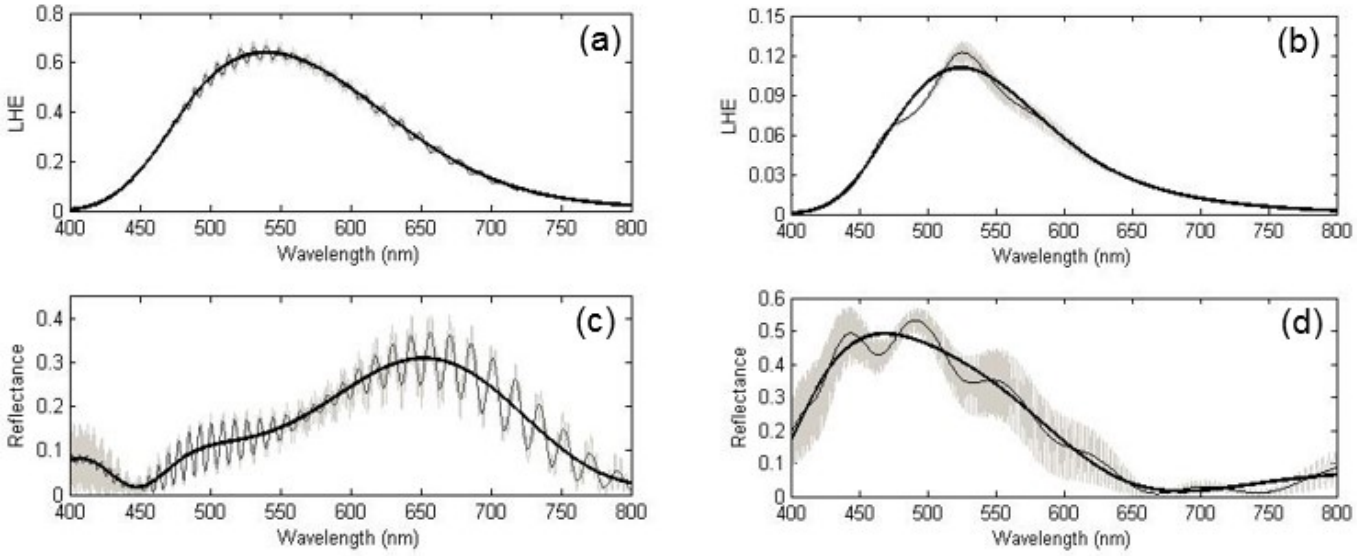

Fig. 5

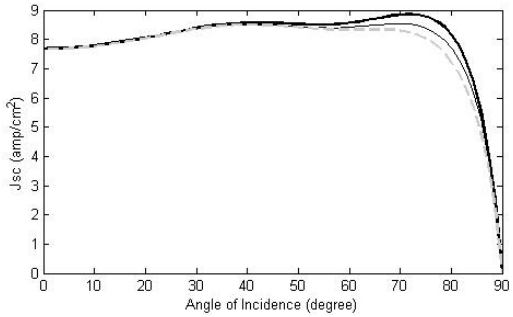

Fig. 6

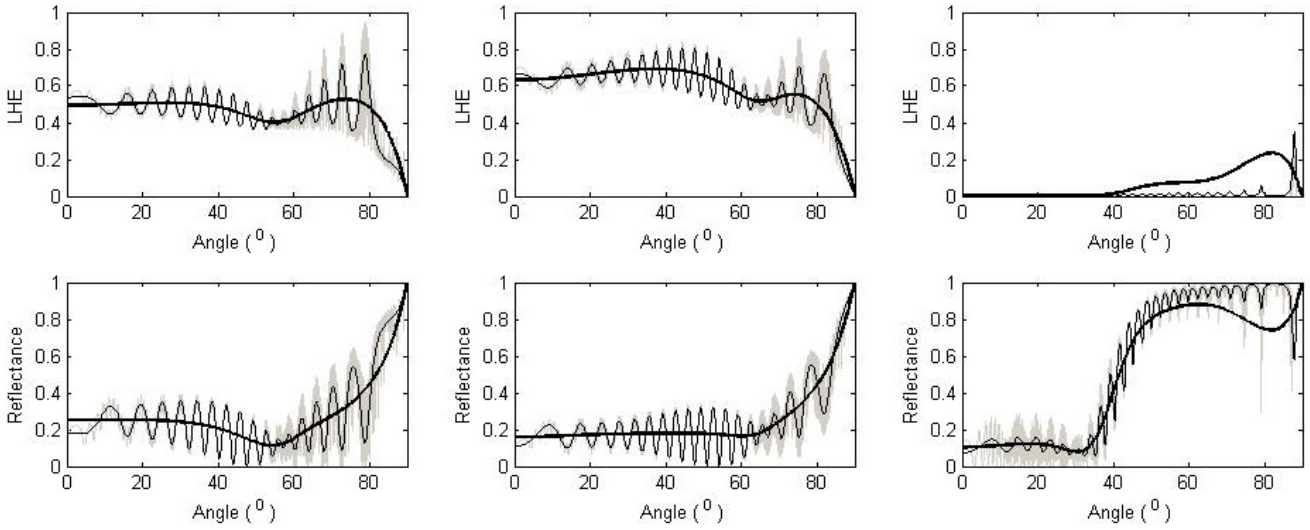

Fig. 7